https://doi.org/10.1016/j.atmosres.2017.09.012

A Macroscopic Physical Model for Self-Initiated Upward Leaders from Tall Grounded Objects and Its Application

Ming-Kit Chan, Mingli Chen* and Ya-ping Du

Department of Building Services Engineering
The Hong Kong Polytechnic University, Hung Hom, Kowloon, Hong Kong.
*Corresponding author: e-mail address: mingli.chen@polyu.edu.hk.

Abstract

This paper presents a macroscopic physical model that can simulate an upward leader initiated from a tall grounded object under thunderclouds. Based on a tri-layer leader channel structure and the energy conservation law, a new equation for estimating the upward leader propagation speed is proposed. Equations for modeling other physical parameters, such as the leader line charge density, leader core radius, leader corona sheath radius, leader current, leader electric field and leader conductance, are also proposed. Besides, a set of initiation and survival criteria for a steady self-initiated upward leader from a tall grounded object is suggested. Based on the suggested criteria and the proposed model, the critical corona and charge amount as well as the minimum height for successful initiation of an upward positive leader (UPL) from a tall grounded object are evaluated and discussed. The model is then used to investigate the general properties of UPLs self-initiated from tall grounded objects with and without the effect of corona space charge layer near the ground under different thunderstorm conditions. The modelling results can well explain the leader properties observed in literature. The model is further tested with two set of experiment data and very promising results are obtained.

Key words: leader initiation, leader propagation, leader modeling, tall grounded object, upward positive leader.

1. Introduction

Lightning interaction with tall structures has been attracting a great deal of attention during last decade. A major reason is the rapid expansion of tall wind power generating stations and high-rise buildings all over the world (*Montanya et al., 2014*). During a thunderstorm, depending on the height of a tall structure, the electric field at the top of the structure may be intensified by tens to a hundred time of that on flat ground, which may cause an air breakdown process hence an upward going leader from the top of the structure. There is a common assumption that if the height of a structure is above 500 m, it only experiences upward discharges (*Diendorfer, 2014*).

A recent study has summed up two types of upward lightning discharge (*Wang and Takagi, 2012*): "self-initiated" one and "other-triggered" one. The self-initiated one refers to those upward discharges initiated at the top of a structure whenever the electric field produced by the thundercloud exceeds a certain level there, while the other-triggered one refers to those initiated also at the top of a structure but due to a sudden polarity change or a big enhancement of the electric field there caused by a nearby lightning activity. The initial stage of an upward lightning discharge is characterized by a leader moving up from the top of the structure towards the thundercloud and a slowly rising continuous current.

Although the upward lightning discharge has been extensively studied base on observations, the inception mechanism of the upward leader is still unclear. To make the things better, various numerical models has been proposed to study the initiation and propagation properties of the upward leader.

Becerra and Cooray (2006a) have recently made a general review of the leader inception models and introduced a self-consistent leader inception and propagation model (SLIM). They have also proposed two simplified models for either static or dynamic leader inception and propagation (*Cooray and Becerra, 2010*). They proposed a stable leader initiation criterion that if the incremental corona charge keeps exceeding a critical value (Q_{crit} = 1 μC), it is considered that a leader starts to propagate with the corona streamer. Although SLIM has been successfully applied to simulate the leader current of an altitude triggered lightning discharge, but the physical basis of this criterion for the stable leader inception is still unclear. For example, a recent laboratory experiment showed that the value of the critical charge (Q_{crit}) was in the range of 0.2 - 0.3 μC with an about 10 μs

stem-to-leader transition time (*Wu et al., 2013*). Another study of long air gap discharge showed that the injected charge is proportional to the leader length with a linear fitting of Q/L = 29.9 μC/m (*Chen et al., 2016*). Different to SLIM, *Rizk (2009)* proposed that the critical streamer or leader corona charge should be proportional to the continuous leader inception voltage ($Q \propto U$), rather than keeping it as a constant. In addition, the electric field and the corona charge around the leader tip must exceed a critical value to maintain leader propagation.

Besides the critical corona charge for the leader inception, the leader propagation behavior is another important issue. Limited by theoretical understandings, most existing models cannot well describe the observed behaviors of upward leader propagations. *Diaz et al. (2015)* have recently reviewed the existing engineering and physical models for positive leaders and compared these models with the long air gap experimental data. However, they have assumed a constant leader speed in their own model. Based on long air gap positive discharge experiment, *Bazelyan et al. (2008)* found that the leader propagation speed (v_L) could be approximated as:

$$v_L \approx a\sqrt{\Delta U_{tip}}, \quad (1)$$

where a = 15 ms^{-1}V$^{-0.5}$ and ΔU_{tip} is the potential difference between the leader tip and the background (the external field). Different from equation (1), *Lalande and Mazur (2012)* suggested to related leader speed with the leader head potential drop as:

$$v_L = v_0(1 - e^{\frac{-2\Delta U_t}{k}}), \quad (2)$$

where ΔU_t is the potential drop ahead of the leader and v_0 a constant.

This study is to introduce a simple macroscopic model for a self-initiated upward leader based on electrostatics rather than the thermos-hydrodynamics (*Gallimberti, 1979)*, aiming at interpretation of leader initiation and propagation behaviors from the point of view of energy conversion and conservation. The overall approach seems like other existing models, but some critical assumptions are different. Specifically, by introducing a tri-layer leader channel structure, a set of equations describing the evolution of the charge, electric field and current, and the size of the leader channel are figured out based on electrostatics; an equation describing the propagation speed of a stable upward leader is derived based on energy conversation law; and a physical criterion for an upward leader inception and stable propagation is proposed and tested.

2. Model Description

A macroscopic model is usually more practical than a microscopic model. For this sake, we aim to model the macroscopic behaviour of an upward leader initiated from a tall grounded structure in terms of the charge, current, electric field and conductivity along the leader channel in the basis of electrostatics. Theoretically, when the local electric field around the top of a tall grounded structure is greater than the breakdown strength of the air, an arcing process hence an upward leader may be initiated there. The input electric energy to the leader is determined by the leader current and the leader channel conductance. The charge transferred hence the leader current highly depends on the background electric field profile established by charges in the thundercloud. Most of the input energy is dissipated in ways of air ionization, heating, optical and electromagnetic emission, as well as the leader channel expansion. In following, we first define the leader channel structure and the electrostatic condition for each part of the channel structure, and then the leader initiation criterion and the leader evolution rule.

2.1. Tri-layer leader channel structure

Although a leader channel structure is complicated, it can be simply separated into three parts: the bright leader tip, the cold streamer zone ahead the leader tip, and the hot conductive channel behind the leader tip. There should be a streamer-to-leader transition zone within the leader tip, where an arcing (breakdown) process converts a streamer into a leader segment. As the arcing process is kept taking place in the leader tip, the leader keeps to grow and extend forward. Based on such a thought, we propose a three-layer leader channel structure as shown in ***Figure 1***, where R_L stands for the conductive leader core radius, R_T the streamer-leader transition zone radius, and R_C the corona streamer sheath radius. Inside the leader core, positive and negative particles can move freely and the radial electric field is nearly zero; Inside the corona sheath, the electric field is assumed to be approximately the critical breakdown electric field, E_C (*Xu and Chen, 2013*); Inside the transition zone, the electrical field is assumed to be brought up gradually from near zero to near E_C; And outside the corona sheath, the electric field gradually reduces to the background electric field level, E_B.

2.2. Assumptions and definitions for parameters in the model

a) We use the sign convention that a positive charge overhead produces a positive electric

field on ground.

b) For simplicity, the upward leader is assumed to propagate along a straight line and it does not branch. The leader gets energy from the background electrical field, E_B, which may include: i) the electric field due to the charges in the cloud, E_{cloud}, ii) that due to the corona space charge layer near the ground, E_{corona}, and iii) that due to the charge transfer by other nearby discharge, E_{other}. That is, $E_B = E_{cloud} + E_{corona} + E_{other}$.

c) Although the thundercloud charge structure is complicated, many measurements show that the vertical electric field under the cloud base is nearly constant (*Stolzenburg et al., 2007*). Hence, the charged cloud may be simplified as a conductive plane with a potential, φ_{cloud} (e.g. -60 MV), at a height, H (e.g. 3000 m), resulting in a constant E_{cloud} (e.g. -20 kV/m) between the cloud base and the ground,

d) The electric field due to the corona space charge layer near the ground, E_{corona}, may be determined based on the observed space electric field profile versus height under a thundercloud, which will be discussed later in section 2.3.

e) The electric field change due to a nearby discharge such as a downward leader, E_{other}, could be either positive or negative and changing with time and space. At a moment when the resulted E_B is not stronger than the leader core longitudinal electric field, E_L, the leader will vanish. A similar phenomenon often occurs in unconnected upward leaders triggered by a downward leader (*Warner, 2012; Gao et al., 2014*), which will be investigated in detail in a separate study.

f) E_B may be enhanced or distorted surrounding the lightning rod or a high-rise structure. If the enhanced electric field around the tip of the rod or the high-rise structure reaches E_C in a certain space range (the critical corona radius: R_{crit}), a leader is supposed to start there. In an other words, a successful leader initiation and stable propagation requires the local electric field around the leader head reaches E_C in a range larger than R_{crit}, which will be discussed in detail in section 2.3.

g) E_L is assumed be uniform along the leader channel and should not be stronger than E_B so that the leader can get energy to grow steadily.

h) We suppose the lightning channel is cylindrically symmetric and extends upward or downward in straight. Therefore, the symmetric cylindrical coordinate system (altitude

z, radius *r*) is adopted, with the ground set as z = 0 and the lightning channel centred along the *z* axis.

2.3. Physics of the model

2.3.1 Leader inception condition

The extend of local electric field enhancement depends on the height and shape of the grounded structure (*Alessandro, 2003; Tan et al., 2013*). We suppose that there is a lightning rod or an equivalent sharp object on the top of the structure, and the leader inception needs the local enhanced electric field around the rod tip (E_{tip}) larger than the critical electric field (E_C) in in a range larger than the critical corona radius (R_{crit}) there. This is:

$$E_{tip} \approx \frac{\int_0^{H_r} E_B(z)dz}{2r} > E_C, \text{ and } \frac{\int_0^{H_r} E_B(z)dz}{E_C} > R_{crit}, \quad (3)$$

where, H_r is the rod tip height above the ground, *r* the lightning rod tip radius, and E_B(z) the background electric field profile without taking account the influence of the structure.

Observations show that the electric field on the ground, E_{ground}, with pointed objects under the thunderstorm is usually not larger than a certain value (*Willett et al., 1999; Biagi et al., 2011*), but might be very high over the sea (*Toland and Vonnegut, 1977*). This property is attributed to the so-called corona space charge layers near the ground. The space charge layer is created on small ground irregularities, such as small objects, grass, bushes, trees, etc. The electric field profile due to the space charge layer varies slowly over time scales of seconds to minutes. As the duration of a lightning leader is within a second, we can assume that the electric field profile is time independent during the leader process. If the corona space charge layer is included, in the case E_{cloud} is larger than E_{ground}, the vertical background field profile can be simply expressed as (*Biagi et al., 2011*):

$$E_B(z) = E_{cloud} + (E_{ground} - E_{cloud})e^{-z/L_c}, \quad (4)$$

where L_c is a characteristic decay height of the corona space charge layer.

Besides, the critical electric field varies with the air density hence the height above sea level (*Chen et al, 2013a*), which can be written as:

$$E_C(z) = E_{C0}e^{-\frac{z}{H_0}}, \quad (5)$$

where E_{C0} (about -750 kV/m and 500 kV/m for negative and positive polarity, respectively)

is the critical electric field at sea level, H_0 is a characteristic height of about 8400 m, and z is the height above sea.

When the local electric field larger than E_C, electrons in the air not only drift opposite to the field, but also ionize the gas and generate an avalanche concurrently. High-energy photons emitted from the primary avalanche provide photoionization in the vicinity, which initiates secondary avalanches. As the local electric field due to electrons in the avalanche keeps comparable to E_C, the avalanche-to-streamer transition may occur and a thin, weakly ionized plasma channel is created, the so-called streamer. As the air temperature increases, a leader with highly ionized and highly conductive (with respect to streamer) plasma channel is created and grows along the path prepared by the preceding streamers. As the local electric field around the leader tip keeps comparable to E_C new streamers can grow from the leader tip and prepare the path for further propagation. If E_B decreases suddenly and significantly or even reverses its polarity, making the local electric field less than E_C, the streamer and leader will vanish.

2.3.2 Leader channel electric field and charge profile

The radial electric field in the leader core (R_L) is assumed to be zero. The radial electric field in the leader transition zone (R_T) is assumed to increase gradually from near zero to the critical electric field there. The radial electric field inside the corona sheath (R_C) is assumed to be equal to the critical electric field there. As a result, the leader channel radial electric field profile, as shown in ***Figure 2***, is given by:

$$E(r) = \begin{cases} 0, & r < R_L \\ \frac{E_C(r-R_L)}{R_T-R_L}, & R_T \geq r \geq R_L \\ E_C, & R_C \geq r \geq R_T \\ \frac{E_C R_C}{r}, & r \geq R_C \end{cases}. \tag{6}$$

The volume charge density versus leader channel radius, as shown ***Figure 3***, is given by:

$$\rho(r) = \frac{\varepsilon_0}{r}\frac{\partial[rE(r)]}{\partial r} = \begin{cases} 0, & r < R_L \\ \frac{\varepsilon_0 E_c\left(2-\frac{R_L}{r}\right)}{R_T-R_L}, & R_T \geq r \geq R_L \\ \frac{\varepsilon_0 E_C}{r}, & R_C \geq r \geq R_T \\ 0, & r > R_C \end{cases}. \tag{7}$$

The line charge density versus leader channel radius, as shown in ***Figure 4***, is given by:

$$\lambda(r) = 2\pi\varepsilon_0 \int_{R_L}^{r} r'\rho(r')dr' = 2\pi\varepsilon_0 \begin{cases} 0, & r < R_L \\ \frac{E_C(r^2 - R_L r)}{R_T - R_L}, & R_T \geq r \geq R_L \\ E_C r, & R_C \geq r \geq R_T \\ E_C R_C, & r \geq R_C \end{cases}. \quad (8)$$

For the volume charge density shown in ***Figure 3***,

$$\rho_1 = \frac{\varepsilon_0 E_c}{R_T - R_L}, \quad \rho_2 = \frac{\varepsilon_0 E_c}{R_T - R_L}\left(2 - \frac{R_L}{R_T}\right), \quad \rho_3 = \frac{\varepsilon_0 E_c}{R_T}. \quad (9)$$

When $R_T >> R_L$, then $\rho_1 \approx \rho_3 = 0.5\rho_2$.

We further hypothesize that the maximum volume charge density (ρ_2) is capped to a limit, then the evolution of the leader transition zone (R_T) is related to that of the leader core radius (R_L). Since the most charges are deposited inside R_C which may be up to several meters larger, the thin-wire approximation should be modified when it is adopted for the leader channel for charge simulations.

2.3.3 Leader head energy conservation

The dynamic variation of the streamer-leader transition zone can be described by a plasma physics model in hydrodynamic scale (*Riousset et al., 2010; Silva and Pasko, 2013*). To evaluate the overall average propagation speed of the leader in an inertial frame, we assume the leader head is a hemispherical ionized gas cloud, which consists of a transition zone shell and a corona sheath shell (streamer zone) with the leader core tip as the center of the hemisphere. Inside the transition zone shell, the electric field increases gradually from the electric field in the leader core (E_L) to that in the corona sheath (E_C). From the conservation of energy and mass for a short moment inside the leader transition zone (dl), we can write:

$$d\left(\frac{1}{2}M{v_{tip}}^2\right) = \left\{Q_T\left[\left(\frac{E_C + E_L}{2} - E_{Dr}\right)\right] - \frac{(P_C + P_R + P_V + P_D)}{v}\right\} dl, \quad (10)$$

where the left-hand term is the total kinetic energy gained in the leader tip transition zone and the right-hand term is the electrical energy injected and energy losses due to heat conduction (P_C) and radiation (P_R), vibration (P_V), and air resistance and friction (P_D). And $E_{Dr} \approx 5.58 \times 10^{-18} \frac{n_e \ln\Lambda}{T_e}$, is the Dreicer field (*Fülöp and Landreman, 2013*), $ln\Lambda$ the Coulomb logarithm, T_e the electron temperature, Q_T the total charges and M the total mass of the leader tip transition zone. For thermal electron-electron collisions with $T_e < 10$ eV, $ln\Lambda$ can be well approximated by $\ln\Lambda \approx 23 - 0.5\ln n_e + 1.5\ln T_e$, where n_e is expressed

in units of cm^{-3} and T_e is expressed in eV.

2.3.4 Leader propagation speed

We assume that inside the leader tip transition zone the heating process is isobaric ($\Delta(VP/T) = 0$) and the total mass is conserved ($\Delta M = 0$). Based on conservation of energy, the gain in kinetic energy of total mass is equal to the difference of the total injected electrical charge energy and the energy losses due to heating, vibration and friction, as shown by equation (10). If the radius of corona sheath shell (streamer zone) around the leader tip keeps larger than R_{crit}, the leader tip transition zone shell as a whole gets more and more kinetic energy as it moves forward within the corona sheath shell by converting a part of the corona sheath shell into a part of conductive leader core step by step, making the leader core extended. As such, the leader tip moving speed is equivalent to the transition zone moving speed, which can be derived from equation (10) as:

$$v_{tip} = \sqrt{\int \frac{F[\eta(E_c+E_L)-2E_{Dr}]}{M} dl}, \quad (11)$$

where, η is coefficient representing the losses of heating, vibration and friction, F = 96485.3365 C/mol is the Faraday constant, and $M = \sum_i (w_i M_i)$ is the effective molar mass among ions composition, within the leader tip transition zone.

For the molar mass M, based on the gas dynamics modelling result (*Aleksandrov and Bazelyan, 1999*), on rainy days, for a positive streamer under standard conditions, $H_3O^+(H_2O)_3$ ions dominate at ground altitudes with a relatively high recombination rate with electrons. Note: $Q_T/M = eN/M = F/M$.

The leader propagation speed is then given by:

$$v_L = \frac{v_{tip}}{1+\tau_d/\tau_a}, \quad (12)$$

where, τ_a and τ_d are the three-body attachment time scale and the delay time for a new leader segment to cross the streamer-to-leader transition zone, respectively. τ_d is also defined as the time needed to heat the leader tip channel up to 5000 K.

Recently, some gas dynamic modeling results (*Riousset et al., 2010; Silva and Pasko, 2013*) have shown that $\tau_d \propto \rho^{-2}$, where ρ is the ambient air density. In the present model, referring to equation (5), we assume that:

$$\tau_d = \tau_{d0} e^{\frac{2z}{H_0}}. \quad (13)$$

2.3.5 Leader corona sheath and conductive core

From equation (8), the leader corona sheath radius (R_C) can simply be related to the leader line charge density (λ_L) by (*Xu and Chen, 2013*):

$$R_C(z) = \frac{\lambda_L(z)}{2\pi\varepsilon_0 E_C(z)}. \quad (14)$$

According to arc discharge experiments, in an ideal thermal balance leader, the energy release rate per unit length keeps a constant as:

$$E_L I_L = \frac{{I_L}^2}{\pi {R_L}^2 \sigma_L} = \frac{{I_L}^2}{g_L} = b, \quad (15)$$

where E_L is the average leader core longitudinal electric field, I_L the leader current, σ_L the conductivity and g_L the conductance of the leader core per unit length, and b a constant of 30 kWm^{-1} (*Bazelyan and Raizer, 2000*).

To maintain thermal equilibrium, when the leader current increases, both the leader core radius and the leader conductivity should increase. Assume that the heating process in the leader core is isobaric and the mass is conservative, i.e. $\Delta(VP/T) = 0$, $\Delta M = 0$, where $V = \pi R_L^2$ the volume, P the pressure and T the temperature of per unit length of the leader core. The temperature is related to the leader core conductivity by $\sigma \propto e^{-C/T}$ (C is a constant) (*Bazelyan and Raizer, 2000*), which means $\Delta\sigma \propto \Delta T$ when $\Delta T << T$. We further assume that the V and P change with T in an equal weighting, then $\sigma_L \propto V^2 \propto R_L^4$ and $g_L = \pi R_L^2 \sigma_L \propto R_L^6$. As a result, the evolution of R_L and σ_L versus g_L can be expressed as:

$$R_L(t) = R_{L0}\left(\frac{g_L(t)}{g_{L0}}\right)^{1/6}, t > 0, \quad (16)$$

where g_{L0} and R_{L0} are the initial leader conductance per meter and the initial leader core radius, respectively. And,

$$\sigma_L(t) = \sigma_{L0}\left(\frac{g_L(t)}{g_{L0}}\right)^{2/3}, t > 0, \quad (17)$$

where $\sigma_{L0} = \frac{g_{L0}}{\pi {R_{L0}}^2}$ is the initial leader core conductivity.

2.3.6 Leader line charge density

The mirror image and charge simulation method (CSM) are applied to calculate the line charge density of the leader channel. CSM is one of the most developed and adopted computational techniques for solving electrostatic problems. The leader development can be divided into many small developing steps ($j = 1, \ldots, N_T$). At each developing step, the

leader core is supposed to extend forward a uniform space length Δl at the leader speed at that moment v_{Lj}, corresponding to a time interval of $\Delta t_j = \Delta l / v_{Lj}$. Thus, at any a moment j, the whole leader channel will include three subsections: a grounded tall object (e.g. a lightning rod) with a height of H_r, a leader channel consisting of a thin conductive core channel surrounded by a thick corona sheath with a length of H_{Lj}, and a hemispheric streamer zone ahead the leader core tip with a length/radius of H_{sj}. The lightning rod is assumed to be thin wire with a radius r_{rod}. The leader channel has a length of $H_{Lj}=j\Delta l$, an spacetime-dependent corona sheath radius of $R_{Cj-1}(z)$, and a time-dependent longitudinal electric field of E_{Lj-1} in its core. The hemispheric streamer zone is supposed to have a length and radius that is equal to the corona sheath radius at the leader tip (z_{tip}), i.e. $H_{sj} = R_{Cj-1}(z_{tip})$, and a radial/longitudinal electric field equal to the critical electric field $E_C(z)$ there. Since the E_{Lj} and $R_{Cj}(z)$ at the present step j are unknown, we will take the E_{Lj-1} and $R_{Cj-1}(z)$ got at the previous step $j-1$ to solve the leader channel charge distributions λ_{ij} at the present step. The solved λ_{ij} is then used to update the E_{Lj} and $R_{Cj}(z)$ as described in next section 2.3.7.

Figure 5 is a schematic diagram to illustrate the usage of CSM to solve the charge distribution problem in an upward leader channel. With the assumption in the above paragraph, at any a step j ($j=1, \ldots, N_T$), the whole channel including the lightning rod, the leader channel and the streamer zone, can be divided into N_j small segments in an equal interval of Δl. The potential difference between the channel centre (along the z axis) and the background at a segment z_k ($k = 1, \ldots, N_j$) is then related to the channel line charge densities λ_{ij} ($i =1, \ldots, N_j$) at other segments by following matrix:

$$\sum_{i=1}^{N_j}(\alpha_{ki} - \alpha'_{ki})\lambda_{ij} = 4\pi\varepsilon_0[\varphi_B(z_k) - \sum_{i=1}^{k} E_i z_i], \tag{18}$$

where

$$\alpha_{ki} = \frac{1}{{r_i}^2}\begin{bmatrix} (z_{i2} - z_k)\left(\sqrt{(z_{i2} - z_k)^2 + r^2} - |z_{i1} - z_k|\right) \\ -(z_{i1} - z_k)\left(\sqrt{(z_{i1} - z_k)^2 + {r_k}^2} - |z_{i1} - z_k|\right) \\ +{r_i}^2 \log\frac{z_{i2}-z_k+\sqrt{(z_{i2}-z_k)^2+{r_i}^2}}{z_{i1}-z_k+\sqrt{(z_{i1}-z_k)^2+{r_i}^2}} \end{bmatrix},$$

$$\alpha'_{ki} = \frac{1}{{r_i}^2}\begin{bmatrix} (z_{i2} + z_k)\left(\sqrt{(z_{i2} + z_k)^2 + {r_k}^2} - |z_{i1} + z_k|\right) \\ -(z_{i1} + z_k)\left(\sqrt{(z_{i1} + z_k)^2 + {r_k}^2} - |z_{i1} + z_k|\right) \\ +{r_i}^2 \log\frac{z_{i2}+z_k+\sqrt{(z_{i2}+z_k)^2+{r_i}^2}}{z_{i1}+z_k+\sqrt{(z_{i1}+z_k)^2+{r_i}^2}} \end{bmatrix},$$

and

$$E_i = \frac{I_{Lj-1}}{g_{rod}}, \quad r_i = r_{rod},\ for\ i = 1\ to\ N_r, lightning\ rod.$$

$$E_i = \frac{b}{I_{Lj-1}}, \quad r_i = R_{Cj-1}(z_i),\ for\ i = N_r + 1\ to\ N_r + j, leader.$$

$$E_i = E_C(z_i),\ r_i = \sqrt{{H_{sj}}^2 - \left(z_i - z_{N_r+j}\right)^2},\ for\ i = N_r + j + 1\ to\ N_j, streamer.$$

$$H_{sj} = R_{Cj-1}\left(z_{N_r+j}\right), N_{sj} = int\left(H_{sj}/\Delta l\right).$$

$$N_r = int(H_r/\Delta l), \quad N_j = N_r + j + N_{sj}.$$

Where, g_{rod} is the conductance per meter of the lightning rod, r_{rod} = 10 mm is the radius of the lightning rod. The α_{ki} and α'_{ki} are the charge and image charge potential coefficients respectively, which are adopted from *Chen et al. (2013a).* The λ_{ij} is the line charge density of the i^{th} segment at the step j, which is to be solved out. The z_{i2} and z_{i1} are the coordinates of the two ends of the i^{th} segment, and $\sum_{i=1}^{k} E_i z_i$ the leader core potential and $\varphi_B(z_k) = \int_0^{z_k} E_B(z)dz$ the background potential for the element z_k.

2.3.7 Leader evolution

Based on the line charge density got from equation (18) for all the whole channel z_i (i =1 to N_j) and the leader speed got from equation (11) for the developing step j (j=1,…,N_T), the evolution of leader core current, electrical field, conductance, leader core and corona sheath (hence the transition zone and streamer zone) radiuses, and core conductivity and temperature behind the leader tip at step j can then be updated iteratively as:

$$I_{Lj} = \lambda_{ij} v_{Lj} = g_{Lj} E_{Lj}, where\ i = Nr + j\ \ is\ the\ leaer\ tip, \tag{19a}$$

$$g_{Lj} = {I_{Lj}}^2/b, \tag{19b}$$

$$E_{Lj} = b/I_{Lj}, \tag{19c}$$

$$R_{Cj}(z_i) = \frac{\lambda_{ij}}{2\pi\varepsilon_0 E_C(z_i)}, i\ =\ Nr + 1 \text{ to } Nr + j, \tag{19d}$$

$$R_{Lj} = \left(\frac{g_{Lj}}{g_{L_0}}\right)^{\frac{1}{6}} R_{L_0}, \tag{19e}$$

$$\sigma_{Lj} = \left(\frac{g_{Lj}}{g_{L_0}}\right)^{\frac{2}{3}} \sigma_{L_0}, \tag{19f}$$

$$T_{Lj} = \left[\frac{1}{T_{L_0}} - \frac{1}{C}\ln\left(\frac{\sigma_{Lj}}{\sigma_{L_0}}\right)\right]^{-1}. \tag{19g}$$

The radius of transition zone R_{Tj} can then be updated according to the core radius R_{Lj} via

Eq. (9), assuming that ρ_2 keeps a constant determined by R_{T0} and R_{L0} values. The time interval at the step j is linked to the space step by $\Delta t_j = \Delta l/v_{Lj}$. As the leader stopping criterion, when $E_{Lj} \geq E_B(z_{tip})$ around the leader tip, the leader will stop moving. In other words, the leader survival condition is:

$$E_{Lj} < E_B(z_{tip}) \text{ or } I_{Lj} > b/E_B(z_{tip}) \text{ or } \lambda_{tip,j} > b/(E_B(z_{tip})v_{Lj}). \quad (20)$$

2.3.8 Critical corona size and charge for a steady leader initiation

At the moment the leader is just initiated (t = 0), as $E_C >> E_L$ and E_{Dr}, the leader initial speed (v_{L0}) in relation to the initial corona length (l_0) can be approximated from equations (11-12) as:

$$v_{L_0} \approx \sqrt{\frac{F\eta E_C l_0}{\mathcal{M}}} / (1 + \frac{\tau_d}{\tau_a}). \quad (21)$$

It is noted that equation (21) can be further approximated as equation (1) by setting $a = \sqrt{\frac{F\eta}{\mathcal{M}}}/(1 + \tau_d/\tau_a)$ and $\Delta U_{tip} = E_C l_0$. This means that equation (1), as an empirical formula for short air gap discharge in lab, can be derived from equations (11-12).

On the other hand, both field observations and lab experiments have showed that the minimum leader speed is not less than 10^4 m/s *(Bazelyan and Raizer, 2000; Wang et al, 2016).* If we set v_{crit}=10^4 m/s as the critical (least) leader starting speed, with the parameters in ***Table 1***, the critical initial corona length at ground level can then be estimated from equation (21) as:

l_0 = 0.105 m ≈ R_{crit}.

Then, if we assume the critical corona sheath radius of leader head is equal to the critical initial coronal length at ground level (R_{crit}), the critical initial corona line charge density at ground level (λ_{crit}) hence the critical charge at ground level (Q_{crit}) can then be estimated from equation (14) as:

$$\lambda_{crit} = 2\pi\varepsilon_0 E_C R_{crit} = 2.91\ \mu\text{C/m}, Q_{crit} = \lambda_{crit} R_{crit} = 0.305\ \mu\text{C}. \quad (22)$$

The Q_{crit} at ground level is about 0.3 μC, which is the upper bound reported in *Wu et al. (2013).* It should be noted that both R_{crit} and λ_{crit} hence Q_{crit} will change with the height of the grounded object, since E_C and τ_d are a function of the height above ground. ***Figure 6*** shows estimates of R_{crit} and Q_{crit} versus initiation height for UPL with the parameters in ***Table 1***. As can be seen from the figure, the R_{crit} and Q_{crit} for ground level are about 0.1 m

and 0.3 μC respectively, and those for 600 m high are about 0.15 m and 0.7 μC respectively. In general, the higher the grounded object is, the larger the R_{crit} and Q_{crit} are.

Furthermore, the minimum (critical) height (H_b) for a grounded object to initiate a steady upward leader under a given E_B profile can be estimated from equation (3) as:

$$(\int_0^{H_b} E_B dz)/E_C(z) \geq R_{crit}. \quad (23)$$

A flowchart is provided in ***Figure 7*** is to illustrate the algorithm of the modelling.

3. Model Applications and Results

3.1. Modeling results for UPL in general

With the parameter values in ***Table 1***, the above model is applied to study the UPL inception under a thundercloud with and without a space charge layer being considered. Two cases are studied:

Case 1. A self-initiated UPL from a grounded object under different E_{cloud} without E_{corona} being considered.

Case 2. A self-initiated UPL from a grounded object under different E_{cloud} with E_{corona} being considered as E_{ground} = -3 kV/m and L_c = 250 m.

In *Case 1*, the space charge layer is neglected. The background electric field just depends on E_{cloud}. With equations (21-23), the minimum self-initiation height (H_b) under different E_{cloud} is evaluated, as shown in ***Figure 8*** and ***Table 2***. The figure and table also include the leader stabilization electric field versus the triggering height estimated with other models (*Rizk, 1994; Lalande et al., 1996; Becerra and Cooray, 2006b*). The results from all these models shown that the triggering height (H_b) is inversely proportional to the background electric field (E_{cloud}). As it is very hard for E_{cloud} to be above -30 kV/m according to observations, we just show the values up to -30 kV/m for comparisons. Our modelling results well match with that of *Lelande et al. (1996),* but have a higher triggering height than others for the same electric field value. This difference is partially due to that we take +500 kV/m as the critical value for the positive breakdown while others take +450kV/m. Meanwhile it also means that the criterion (E_{crit} and v_{crit}, hence the R_{crit} and Q_{crit}) for self-triggered UPL in the present model is stricter than that in other models. Nevertheless, our results well match the usual assumption that a structure with a height less than 100 m is struck only by downward lightning.

In *Case 2*, we have modified our model with a changing background electric field by taking account a corona space charge layer near ground. The background electric field profile is based on equation (4). By choosing an adequate L_c, equation (4) can well match with observed space electric field profiles in literature. Taking E_{ground} = -3 kV/m and L_c = 250 m, H_b versus E_{cloud} is also evaluated, as shown in ***Figure 8*** and ***Table 2***. As can be seen from both the figure and the table, the minimum self-initiation height becomes larger when the space charge layer is considered. For example, for E_{cloud} = -20 kV/m the minimum initiation height is only 252.5 m in *Case 1* but becomes 410 m in *Case 2*. This is because that the background electric field produced by the thundercloud is weakened by the corona space charge layer near ground. In general, the minimum self-initiation height strongly depends on the actual E_{cloud} and E_{ground} values, and the results here are comparable to those in *Aleksandrov et al. (2005)*.

Table 3 is a summary of simulation results of the current, speed, channel size, conductivity and temperature of an UPL propagating from its initiation height (H_b) up to 3000 m high under different E_{cloud}, for both *Case 1* and *Case 2*. The results show that while the initial leader velocity is fixed at 10^4 m/s, initial values of all the leader current, line charge density and corona sheath size are inversely proportional to the background electric field (E_{cloud}) and positively proportional to the initiation height (H_b). The final values of all these parameters are dependent on the leader propagation length (3000 m – H_b). The results also show that UPLs self-initiated at different heights exhibit different speed evolution mode. Such a phenomenon has already been mentioned in a recent observation in Japan (*Wang and Takagi, 2012*). Other observations (*Kito et al., 1985; Asakawa et al., 1997; Wada et al., 2003*) have reported the speed of UPLs ranging from 6×10^4 to 1.4×10^6 m/s. Our simulation results (1.0×10^4 to 7.3×10^5 m/s) are within this range.

In following, we select the case of E_{cloud} = -20 kV/m as an example to illustrate the details of the evolution of each of the leader parameters.

Shown in ***Figures 9a*** and ***10a*** are evolutions of the leader charge density and the corona sheath radius respectively, for E_{cloud} = -20 kV/m for *Case 1*. As seen from the figures, while the leader is growing, more and more electric charges accumulate along the channel. This is because that the potential difference between the leader core and the environment keeps increasing as the leader extends upward. The figures also show that at the beginning stage

(t_0) the leader tip charge density is higher than that at stage t_1, while that at stage t_1 is smaller than that at stage t_2 and so on. This is due to that the grounded object is supposed to be a good conductor and the voltage drop along it is very small, while the leader channel has limited conductance and voltage drop alone it is relatively big. The corresponding evolutions of the leader charge density and the corona sheath radius for E_{cloud} = -20 kV/m for *Case 2* are shown in ***Figures 9b*** and ***10b***, respectively. Their evolution trends are very similar to those for *Case1*, except the difference in the initiation height due to the effect of the corona space charge layer.

Since the similarity between *Case 1* and *Case 2*, in following we just present detailed results for E_{cloud} = -20 kV/m for *Case 2*, for the leader speed (***Figurer 11***), leader current and longitudinal electric field (***Figurer 12***), leader core conductance and conductivity (***Figure 13***), leader core and transition zone radius (***Figurer 14***), and the leader core temperature (***Figurer 15***), for discussions.

As seen from ***Figure 11***, the leader shows first a continuous accelerating from the initial speed of 10^4 m/s when at its initiation height of 410 m up to about 7×10^5 m/s when it reaches the height of about 2000 m and then a deaccelerating to about 6.7×10^5 m/s when it reaches the height of 3000 m. This is because that the delay time (τ_d) for a new leader segment to cross the stream-to-leader transition region increases with the propagating height. In other words, the required streamer-leader heating time is longer at a lower pressure than that at a higher pressure. The feature of evolution of leader speed for other cases is similar to this case.

The leader current (***Figure 12***) keeps increasing from the initial value of about 1.8 A up to about 308 A, while the longitudinal electric field keeps decreasing from the initial value of about -16.7 kV/m down to about -100 V/m, as the leader propagates from the initiation height of 410 m up to 3000 m high

The conductance (***Figure 13***), radius (***Figure 14***) and temperature (***Figure 15***) of the leader core increase from their initial values of 10 mS per meter, 1 mm and 4000 K respectively up to about 3.1 S per meter, 5.6 mm and 9500 K respectively, as the leader propagates from the initiation height of 410 m up to 3000 m high. ***Figure 14*** also shows that while the leader core radius (R_L) keeps expanding, the leader streamer-core transition zone radius (R_T =10~12 mm) does not change too much.

3.2. Model validation with experiment data

Two sets of experiment data in literature have been chosen to validate the model.

Experiment 1: an UPL in a rocket-triggered lightning discharge reported in *Chen et al. (2013b)*. It is the initial UPL in a classical rocket-triggered lightning discharge succeeded on 2 August 2005 during SHATLE [*Qie et al*., 2009]. Measurements of the leader included the channel base currents and high-speed camera images. The initiation height of the leader was estimated at 266.4 m above the ground, and the final height viewed by the camera was about 602.4 m above the ground.

To simulate the UPL in *Experiment 1*, following initial model parameters are adopted: E_{cloud} = -31.75 kV/m with E_{ground} = -3 kV and L_c = 250 m, R_{L0} = 1 mm, η = 0.046. Other initial model parameters are the same to ***Table 1***. It should be mentioned that the model initial parameters like η and $\mathcal{M}$ might be case dependent. They can be fine-tuned to better match with observations when necessary. Comparisons of the leader current and leader speed between the model-based and experiment -based estimates are shown in ***Figure 16*** and ***Figure 17***, respectively. Other leader parameters like the leader line charge density, leader core electric field and conductance, leader core and corona sheath radiuses, as well as the leader core temperature are also modeled, which are not shown here for conciseness. The modelled leader currents and speeds well match with the experiment data, indicating that the model well describe the relationships between the background electric field (E_B), leader initiation height (H_b) and propagation speed (v_L), and leader current (I_L) and charge deposit (λ_L).

Experiment 2: a positive point-to-plane air gap discharge reported in *Zhou et al*. (2015). The discharge was made for a 0.93 m point-plane gap under a positive IEC standard switching impulse voltage (250/2500 μs) with the amplitude of about 350 kV. In the experiment, a 4 m optical path Mach-Zehnder interferometer was set up to observe the gas density variation and radial expansion of leader discharges. Theoretically, a leader discharge is an isobaric process (*Riousset et al., 2010; Silva and Pasko, 2013*). By the ideal gas law, a high temperature leader can reduce the gas density and change the refractive index of the air. Their results show that the estimated diameter of the leader channels is expanded from 1.5 mm to 3.5 mm and the average expansion speed is about 6.7 m/s.

To simulate the point-to-plane gap discharge in *Experiment 2*, a uniform E_B of -350 kV/m is assumed to match with that in the experiment. A 1-m high metallic rod with a radius 1 cm placed on a grounded plane and a plane-to-plane gap of 6.5 m is assumed so that the modeled leader propagation time matches with the leader heating time period in the experiment. Since the major purpose is to evaluate the evolution trend of leader core radius as describe by equation (19d) of the model with the experiment, three different initial values (d_0 = 1 mm, 1.5 mm and 2 mm) of leader core diameter are tried with the model. Other initial parameters are the same to those in ***Table 1.*** Shown in ***Figure 18*** is a comparison of the leader core diameter between the modeled and measured results for *Experiment 2*. As can be seen from the figure, the evolution trend of modeled leader core diameter with d_0 = 1.5 mm is well consistent with that of the experiment, indicating that the equation (19d) well describes the leader core evolution trend. Other parameters such as the leader current, leader speed, leader charge and core conductance are also modeled but not shown here for conciseness.

4. Summary and Discussion

A macroscopic physical model for self-initiated upward leaders from tall grounded objects has been proposed. In comparison with other models, such as the SILM (*Becerra and Cooray, 2006; Gallimberti et al., 2002; Cooray and Becerra, 2010*), the main points of the present model can be summarized as following:

a) The leader channel is consisted of three layers, a thin conductive core surrounded by a transitional zone and a thick corona charge sheath;
b) The first leader segment is created when the electric field enhancement around tip of a grounded object reaches the critical breakdown electric field in a certain range;
c) The leader speed is subjected to the law of energy and mass conservation inside the streamer-to-leader transitional zone around the leader head;
d) A steady leader requires that the leader initial speed (energy) should be not less than the minimum (critical) speed observed for leaders in both field and lab experiments, which corresponding to a critical corona sheath radius hence a critical corona sheath charge ahead the leader.
e) The leader charge distribution observes the Poisson's equation and follows the

charge simulation method;

f) The leader survives when its channel electrical field is less than the background electric field and the streamer zone ahead the leader is no less than the critical corona length required there.

The model has been applied to study UPL inceptions from tall structures under different thunderclouds with and without the corona space charge layer effect. Based on the leader initiation criterion in the model, the critical corona sheath length and corona charge as a function of the leader initiation height and the minimum leader initiation height as a function of the thundercloud condition for UPL are estimated and discussed. Evolutions of the speed, charge distribution, current, electric field, conductance and conductivity, channel size and temperature of UPL under different thundercloud conditions are also obtained and discussed. In addition, the model is tested with two sets of experiment data and the results are promising.

Although the present model is simple, in the sense that it does not consider the details of thermal gas dynamics inside the leader channel, it works well in the prediction of main parameters of an UPL initiated from grounded objects. As about the application, the model could be used to analyze the incidence and probability of upward lightning to a given tall structure based on the statistics of the ground electric field or vertical electric profile in the area the structure is located. With analyzing results, one optimizes the protection measures for effective protection, such as the optimal mast/lightning rod height etc. Furthermore, without considering the stepwise behavior, the present model can also be modified to simulate a downward leader and its attachment to an upward connecting leader by reversing the propagation direction and changing the values of the simulation parameters accordingly. By statistical analysis of the attachment to a given tall structure under various downward lightning events, one can estimate accurately the striking distance versus the lightning strength for the given tall structure.

Acknowledgments

Works leading to this paper is supported by the Research Committee of The Hong Kong Polytechnic University and the Research Grant Council of Hong Kong Government (Grant No.: PolyU 5123/12E).

References

Aleksandrov, N.L., and E.M. Bazelyan (1999). Ionization processes in spark discharge plasmas. *Plasma Sources Sci. T.*, 8, 285–294.

Aleksandrov, N.L., E.M. Bazelyan, and Y.P. Raizer (2005). Initiation and development of first lightning leader: the effects of coronae and position of lightning origin. *Atmos. Res.*, 76, 307 – 329. DOI:10.1016/j.atmosres.2004.11.007.

Alessandro, F. D. (2003). The use of 'Field Intensification Factors' in calculations for lightning protection of structures. *J. Electrostat.*, 58, 17-43. DOI:10.1016/S0304-3886(02)00178-X.

Asakawa, A., K. Miyake, S. Yokoyama, T. Shindo, T. Yokota, T. Sakai (1997). Two types of lightning discharges to a high stack on the coast of the Sea of Japan in winter. *IEEE Trans. Power Del.*, 12, no.3, 1222–1231. DOI:10.1109/61.636953.

Bazelyan, E.M., and Y.P. Raizer (2000). Lightning Physics and Lightning Protection. *Institute of Physics Publishing, Philadelphia*.

Bazelyan, E.M., Y.P. Raizer, and N.L. Aleksandrov (2007). The effect of reduced air density on streamer-to-leader transition and on properties of long positive leader. *J. Phys. D: Appl. Phys.*, 40, 4133–4144.

Bazelyan, E.M., Y.P. Raizer, and N.L. Aleksandrov (2008). Corona initiated from grounded objects under thunderstorm conditions and its influence on lightning attachment. *Plasma Sources Sci. T.*, 17, 024015.

Becerra, M., and V. Cooray (2006a). A self-consistent upward leader propagation model. *J. Phys. D: Appl. Phys.*, 39, 3708–3715.

Becerra, M. and V. Cooray (2006b), A simplified physical model to determine the lightning upward connecting leader inception, *IEEE Trans. On Power Delivery*, 21, No.2, 897-908.

Biagi, C. J., M.A. Uman, J. Gopalakrishnan, J.D. Hill, V.A. Rakov, T. Ngin, D.M. Jordan (2011). Determination of the electric field intensity and space charge density versus height prior to triggered lightning. *J. Geophys. Res.*, 116, D15201. DOI:10.1029/2011JD015710.

Chen, M., X. Gou, Y. Du (2013a). The effect of ground altitude on lightning striking distance based on a bi-directional leader model. *Atmos. Res.*, 125, 76-83. DOI:10.1016/j.atmosres.2012.08.019.

Chen, M., D. Zheng, Y. Du, Y. Zhang (2013b). Evolution of line charge density of steadily-developing upward positive leaders in triggered lightning, *J. Geophys. Res. Atmos.*, 118, 4670–4678. DOI:10.1002/jgrd.50446.

Chen, S., R. Zeng, C. Zhuang, X. Zhou, Y. Ding (2016). Experimental Study on Branch and Diffuse Type of Streamers in Leader Restrike of Long Air Gap Discharge. *Plasma Sci. T.*, 18, no.3.

Cooray, V., M. Becerra (2010). Attachment of lightning flashes to grounded structures, *Ch. 4 in Lightning Protection, IET, London*, 165-268. DOI:10.1049/PBPO058E_ch4.

Da Silva, C. L., V.P. Pasko (2013). Dynamics of streamer-to-leader transition at reduced air densities and its implications for propagation of lightning leaders and gigantic jets. *J. Geophys. Res. Atmos.*, 118, 13561–13590. DOI:10.1002/2013JD020618.

Diaz, O., L. Arevalo, V. Cooray (2015). Leader channel models for long air positive electrical discharges. *J. Electrostat.*, 76, 208-215. DOI:10.1016/j.elstat.2015.05.026.

Diendorfer, G. (2014). Tower initiated lightning discharges, *Ch. 7 in The Lightning Flash 2nd edition, IET, London*, 41-229. DOI:10.1049/PBPO069E_ch7.

Fülöp, T., M. Landreman (2013). Ion Runaway in Lightning Discharges. *Phys. Rev. Lett.*, 111, 15006. DOI:10.1103/PhysRevLett.111.015006.

Gallimberti, I. (1979). The mechanism of long spark formation. *J. Physique. Physique Coll*, 40, 193–250.

Gallimberti, I., G. Bacchiega, A. Bondiou-Clergerie, P. Lalande (2002). Fundamental processes in long air gap discharges. *C. R. Physique*, 3, 1–25.

Gao, Y., W. Lu, Y. Ma, L. Chen, Yang Zhang, X. Yan, Y. Zhang (2014). Three-dimensional propagation characteristics of the upward connecting leaders in six negative tall-object flashes in Guangzhou. *Atmos. Res.* 149, 193 – 203. DOI:10.1016/j.atmosres.2014.06.008.

Kito, Y., K. Horii, Y. Higashiyama, K. Nakamura (1985). Optical aspects of winter lightning discharges triggered by the rocket-wire technique in Hokuriku district of Japan, *J. Geophys. Res.*, 90(D4), 6147–6157. DOI:10.1029/JD090iD04p06147.

Lalande, P. (1996), Study of the lightning stroke conditions on a grounded structure, *Doctoral Thesis*, A publication of Office National d'Etudes et de Recherches A'erospatiales (ONERA).

Lalande, P., V. Mazur (2012). A Physical Model of Branching in Upward Leaders. *J. Aerospace Lab*, 5.

Montanyà, J., O. van der Velde, E.R. Williams (2014). Lightning discharges produced by wind turbines. *J. Geophys. Res. Atmos.*, 119, 1455–1462. DOI:10.1002/2013JD020225.

Qie, X., Y. Zhao, Q. Zhang, J. Yang, G. Feng, X. Kong, Y. Zhou, T. Zhang, G. Zhang, T. Zhang, D. Wang, H. Cui, Z. Zhao, and S. Wu (2009), Characteristics of triggered lightning during Shandong artificial triggering lightning experiment (SHATLE), *Atmos. Res.*, 91, 310-315.

Riousset, J.A., V.P. Pasko, A. Bourdon (2010). Air-density-dependent model for analysis of air heating associated with streamers, leaders, and transient luminous events. *J. Geophys. Res.*, 115, A12321. DOI:10.1029/2010JA015918.

Rizk, F.A.M. (1994b), Modeling of Lightning Incidence to Tall Structures, Part I: Application, *IEEE Trans. Power Del.*, 9, No. 1, 172 -178.

Rizk., F.A.M. (2009). Modeling of Lightning Exposure of Buildings and Massive Structures. *IEEE Trans. Power Del.*, 24, no.4. DOI:10.1109/TPWRD.2009.2028759.

Stolzenburg, M., T.C. Marshall, W.D. Rust, E. Bruning, D.R. MacGorman, T. Hamlin (2007). Electric field values observed near lightning flash initiations. *Geophys. Res. Lett.*, 34, L04804. DOI:10.1029/2006GL028777.

Tan, Y., X. Guo, J. Zhu, Z. Shi, D. Zhang (2013). Influence on simulation accuracy of atmospheric electric field around a building by space resolution. *Atmos. Res.*, 134, 301-307. DOI:10.1016/j.atmosres.2013.11.023.

Toland, R.B., B. Vonnegut (1977). Measurement of maximum electric field intensities over water during thunderstorms. *J. Geophys. Res.*, 82(3), 438–440. DOI:10.1029/JC082i003p00438.

Wada, A., A. Asakawa, T. Shindo, S. Yokoyama (2003). Leader and return stroke speed of upward-initiated lightning. *Int. Conf. Atmos. Electricity (ICAE 2003)*, paper C3-20.

Wang, D., N. Takagi (2012). Characteristics of winter lightning that occurred on a windmill and its lightning protection tower in Japan. *IEEJ Trans. Power Energy*, 132, no.6, 568–572. DOI:10.1541/ieejpes.132.568.

Wang, X., J. He., Z. Yu., R. Zeng, F. Rachidi (2016). Influence of ground wire on the initiation of upward leader from110 to 1000 kV AC phase line. *Electr. Power Syst. Res.*, 130, 103-112. DOI:10.1016/j.epsr.2015.08.022.

Warner, T.A. (2012). Observations of simultaneous upward lightning leaders from multiple tall structures. *Atmos. Res.*, 117, 45–54. DOI:10.1016/j.atmosres.2011.07.004.

Willett, J.C., D.A. Davis, P. Laroche (1999). An experimental study of positive leaders initiating rocket-triggered lightning. *Atmos. Res.*, 51, 189–219. DOI:10.1016/S0169-8095(99)00008-3.

Wu, C., S. Xie, F. Qi, B. Li, J. Wan, J. He (2013). Effect of corona discharges on the inception of positive upward leader-streamer system. *Int. J. Mod. Phys. B*, 27, 1350165. DOI:10.1142/S0217979213501658.

Xu, Y., M. Chen (2013). A 3D self-organized leader propagation model and its engineering approximation for lightning protection analysis. *IEEE Trans. Power Del.*, 28, no.4. DOI:10.1109/TPWRD.2013.2263846.

Zhou, X., R. Zeng, C. Zhuang, S. Chen (2015). Experimental study on thermal characteristics of positive leader discharges using Mach-Zehnder interferometry. *Phys. Plasmas*, 22, 63508. DOI:10.1063/1.4922660.

Captions

Figure 1. Sketch of a tri-layer upward leader channel structure induced on the metallic grounded structure (not to scale). The grey color in the figure represents the region of the streamer zone and green color the region of the leader tip. The double arrow symbol indicates the rough thickness of the layer.

Figure 2. The radial electric field profile in a tri-layer leader channel (not to scale).

Figure 3. The radial volume charge density profile in a tri-layer leader channel (not to scale).

Figure 4. The radial line charge density profile in a tri-layer leader channel (not to scale).

Figure 5. For modelling leader charge distribution with CSM: (a) The leader channel is equivalent to a cylindrically symmetric corona sheath surrounding a thin conductive core with the corona sheath radius varies with time and height; (b) The channel is divided into many small segments each with an equal length.

Figure 6. The critical corona length (R_{crit}) and charge (Q_{crit}) versus the initiation height for a successful UPL initiation.

Figure 7. Flowchart of the leader modelling algorithm at each space/time step j.

Figure 8. Minimum UPL self-triggering height versus cloud electric field (E_{cloud}) with (dashed-line) and without (solid-line) a space charge layer from the present model, and the leader stabilization field versus triggering height from other models (also see Table 2).

Figure 9. Spatial and temporal evolution of the leader line charge density (λ_L). (a) for Case 1 for E_{cloud} = -20 kV/m, (b) for Case 2 for E_{cloud} = -20 kV/m and E_{ground} = -3 kV/m.

Figure 10. Spatial and temporal evolution of the leader corona sheath radius (R_C). (a) for Case 1 for E_{cloud} = -20 kV/m, (b) or Case 2 for E_{cloud} = -20 kV/m and E_{ground} = -3 kV/m.

Figure 11. Leader speed (v_L) versus propagation time (top) and that versus leader tip height (below), for Case 2 for E_{cloud} = -20 kV/m and E_{ground} = -3 kV/m.

Figure 12. Leader current (I_L in blue) and leader electric field (E_L in brown) versus propagation time for Case 2 for E_{cloud} = -20 kV/m and E_{ground} = -3 kV/m.

Figure 13. Leader channel conductance per meter length (g_L in blue) and conductivity (σ_L in brown) versus leader propagation time, for Case 2 for E_{cloud} = -20 kV/m and E_{ground} = -3 kV/m.

Figure 14. Leader core radius (R_L solid line) and transition layer radius (R_T dash line) versus leader tip height for Case 2 for E_{cloud} = -20 kV/m and E_{ground} = -3 kV/m.

Figure 15. Leader core temperature (T_L) versus leader propagation time (left) and that versus leader tip height (right), for Case 2 for E_{cloud} = -20 kV/m and E_{ground} = -3 kV/m.

Figure 16. Comparison of the leader current evolution between modeled (solid-line) and observed (dashed-line) results for the UPL reported in *Chen et al. (2013b)*.

Figure 17. Comparison of the leader speed evolution between modeled (solid-line) and observed (short-dashed-line) results for the UPL reported in *Chen et al. (2013b)*. Long-dashed-line is the model-based averaged speed for different channel segments in accordance with the observed result.

Figure 18. Evolution trends of the leader core diameter modeled with different initial values (1, 1.5 and 2 mm respectively) and that measured in lab, for the point-to-plane gap discharge reported in *Zhou et al. (2015)*.

Table 1. Initial parameters for the upward positive leader simulation.

Table 2. The minimum UPL self-triggering height versus cloud electric field (E_{cloud}) for both Case 1 and Case 2 from the present model, and the leader stabilization field versus triggering height from other models (also see Figure 8).

Table 3. Summary of simulation results for UPL traveling from its triggering height (H_b) to 3000 m high with different cloud electric field (E_{cloud}) for both Case 1 and Case 2.

1

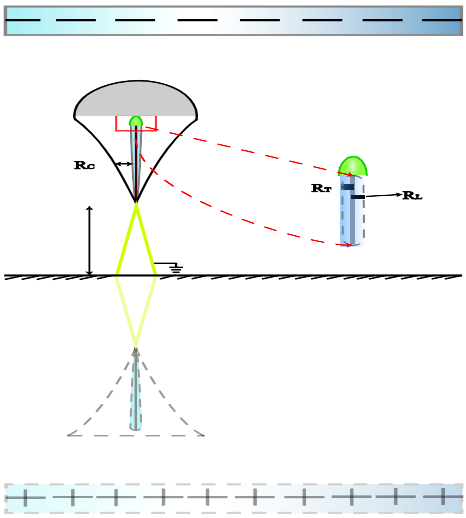

Figure 1. Sketch of a tri-layer upward leader channel structure induced on the metallic grounded structure (not to scale). The grey color in the figure represents the region of the streamer zone and green color the region of the leader tip. The double arrow symbol indicates the rough thickness of the layer.

2

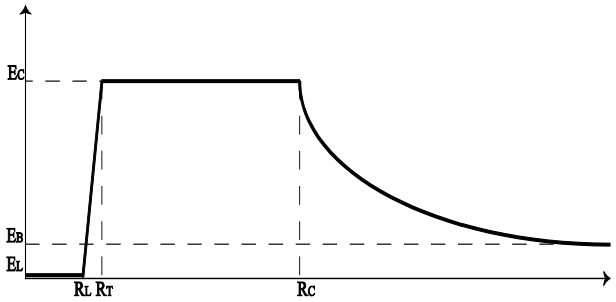

Figure 2. The radial electric field profile in a tri-layer leader channel (not to scale).

3

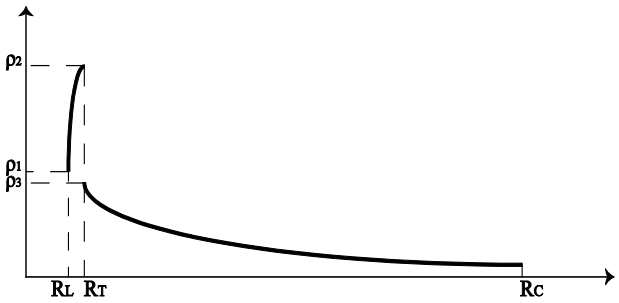

Figure 3. The radial volume charge density profile in a tri-layer leader channel (not to scale).

4

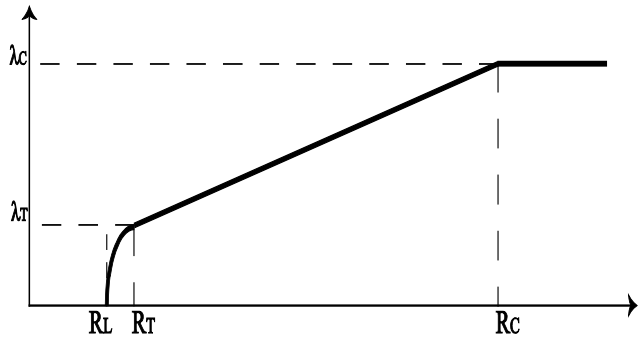

Figure 4. The radial line charge density profile in a tri-layer leader channel (not to scale).

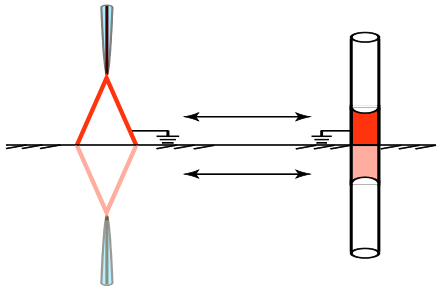

(a)

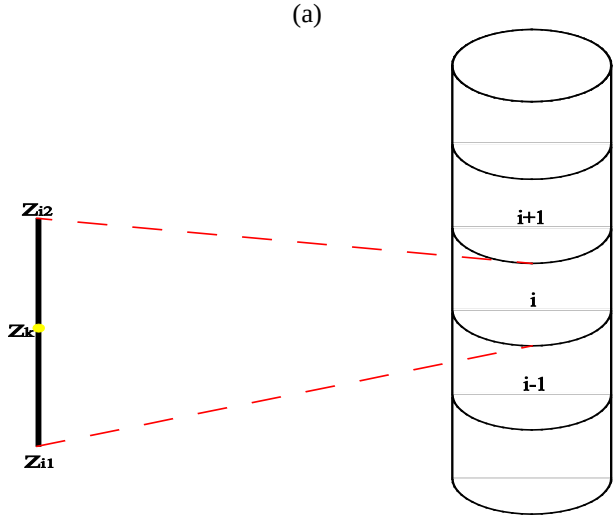

(b)

Figure 5. For modelling leader charge distribution with CSM: (a) The leader channel is equivalent to a cylindrically symmetric corona sheath surrounding a thin conductive core with the corona sheath radius varies with time and height; (b) The channel is divided into many small segments each with an equal length.

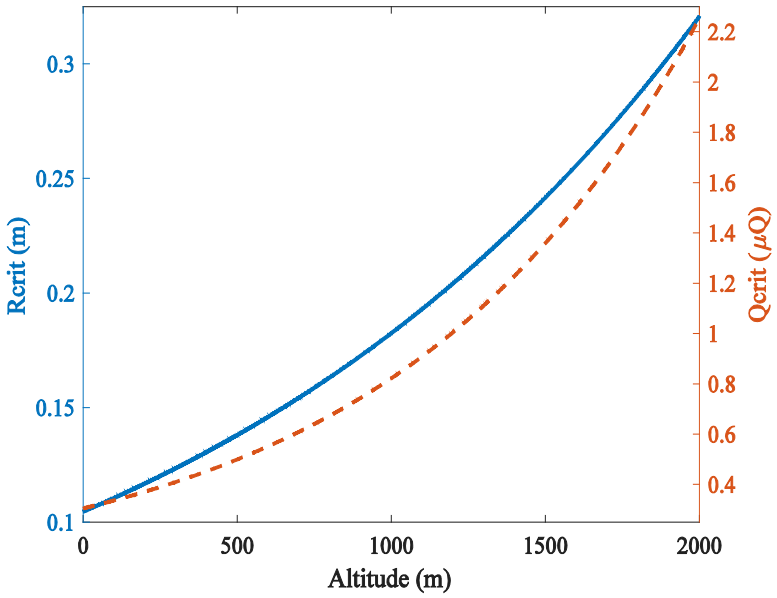

Figure 6. The critical corona length (R_{crit}) and charge (Q_{crit}) versus the initiation height for a successful UPL initiation.

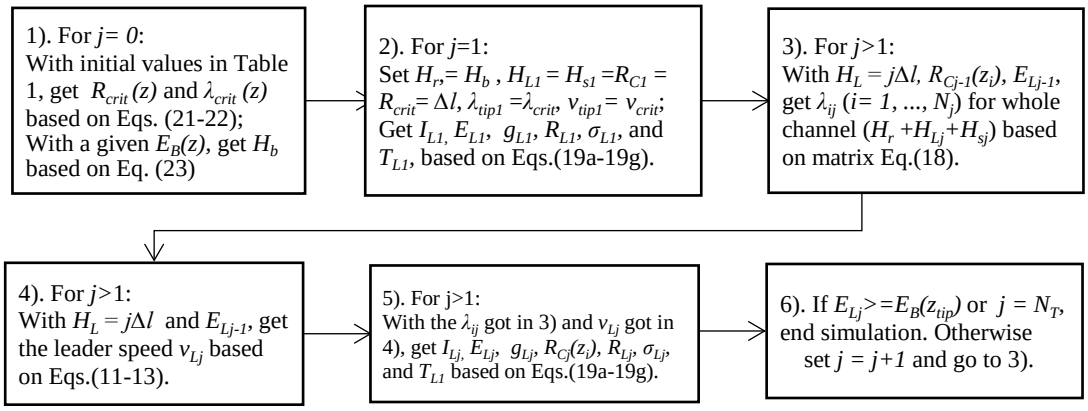

Figure 7. Flowchart of the leader modelling algorithm at each space/time step j.

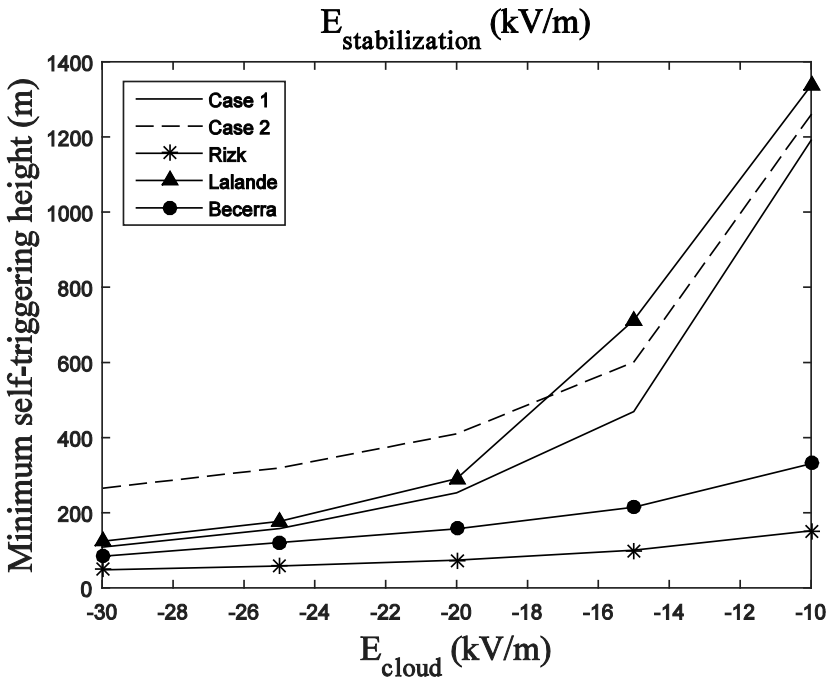

Figure 8. The minimum UPL self-triggering height versus cloud electric field (E_{cloud}) with (dashed-line) and without (solid-line) a space charge layer from the present model, and the leader stabilization field versus triggering height from other models (also see ***Table 2***).

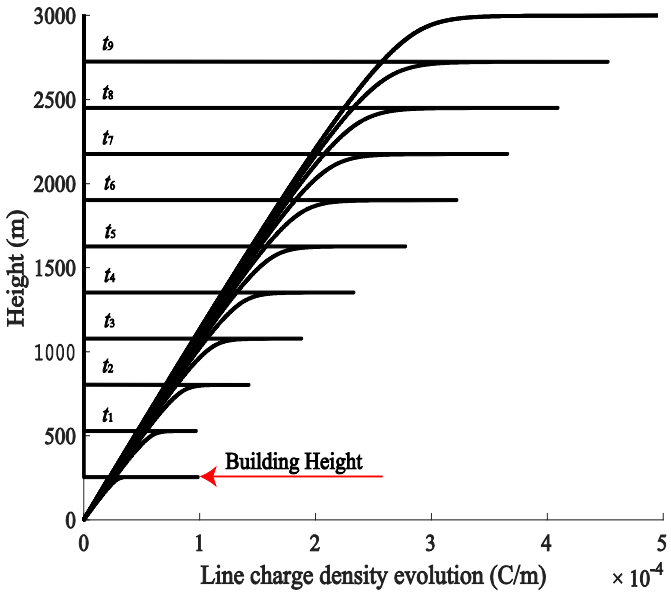

(a)

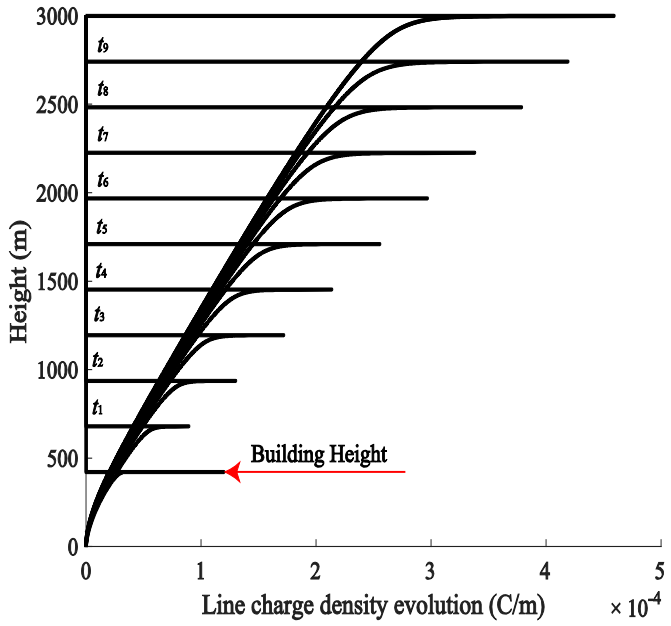

(b)

Figure 9. Spatial and temporal evolution of the leader line charge density (λ_L). (a) for Case 1 for E_{cloud} = -20 kV/m, (b) for Case 2 for E_{cloud} = -20 kV/m and E_{ground} = -3 kV/m.

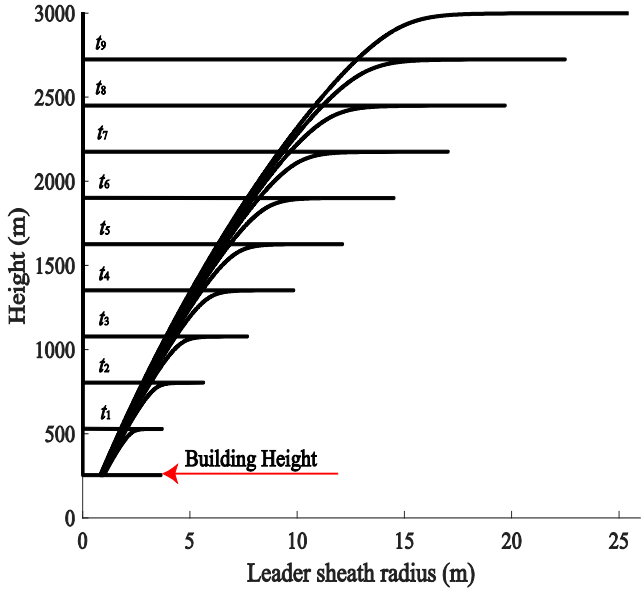

(a)

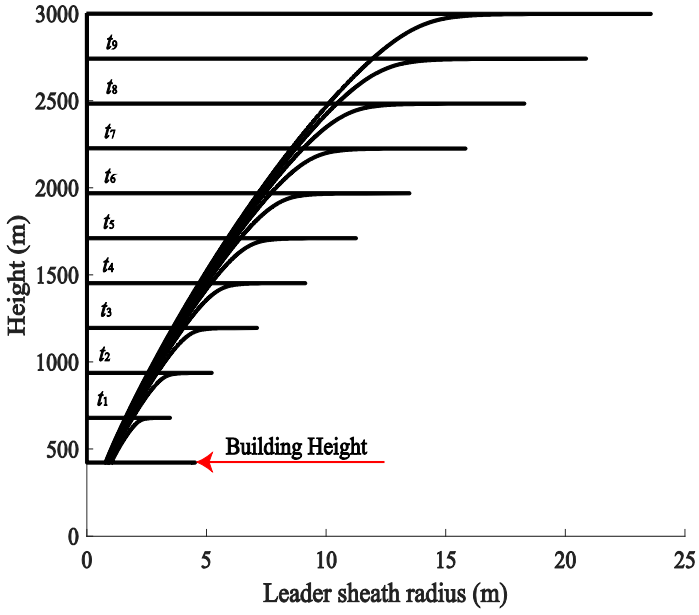

(b)

Figure 10. Spatial and temporal evolution of the leader corona sheath radius (R_C). (a) for Case 1 for E_{cloud} = -20 kV/m, (b) or Case 2 for E_{cloud} = -20 kV/m and E_{ground} = -3 kV/m.

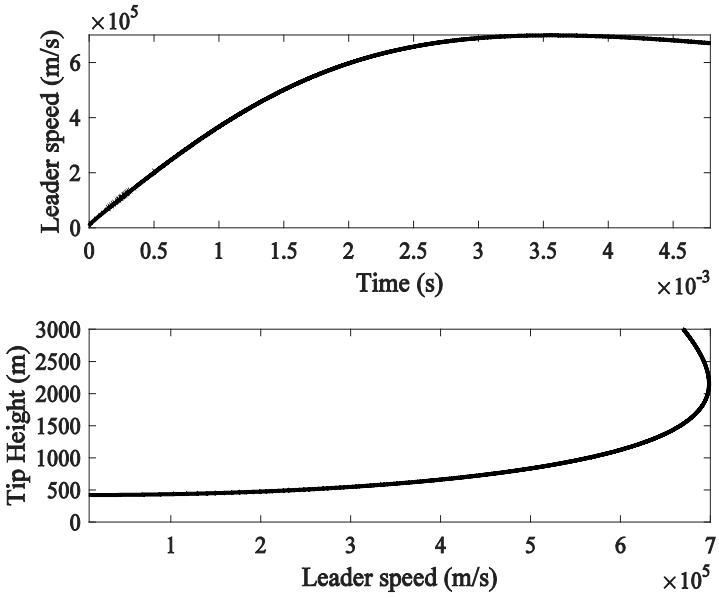

Figure 11. Leader speed (v_L) versus propagation time (top) and that versus leader tip height (below), for Case 2 for E_{cloud} = -20 kV/m and E_{ground} = -3 kV/m.

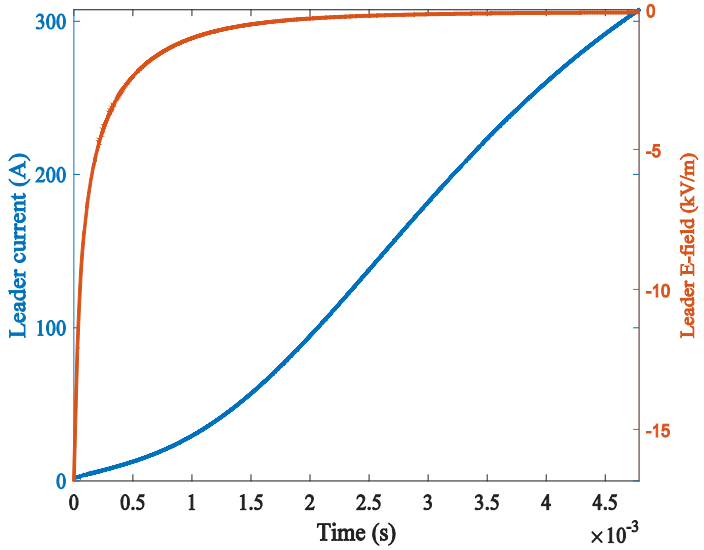

Figure 12. Leader current (I_L in blue) and leader electric field (E_L in brown) versus propagation time for Case 2 for E_{cloud} = -20 kV/m and E_{ground} = -3 kV/m.

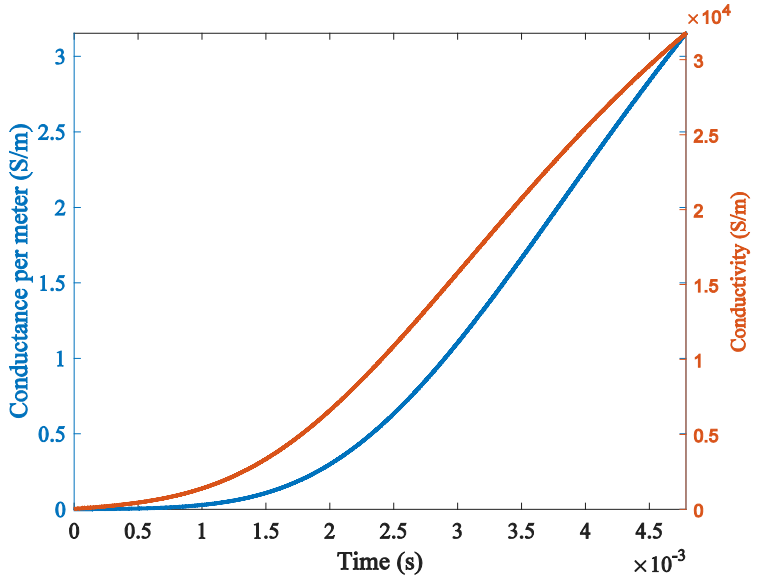

Figure 13. Leader channel conductance per meter length (g_L in blue) and conductivity (σ_L in brown) versus leader propagation time, for Case 2 for E_{cloud} = -20 kV/m and E_{ground} = -3 kV/m.

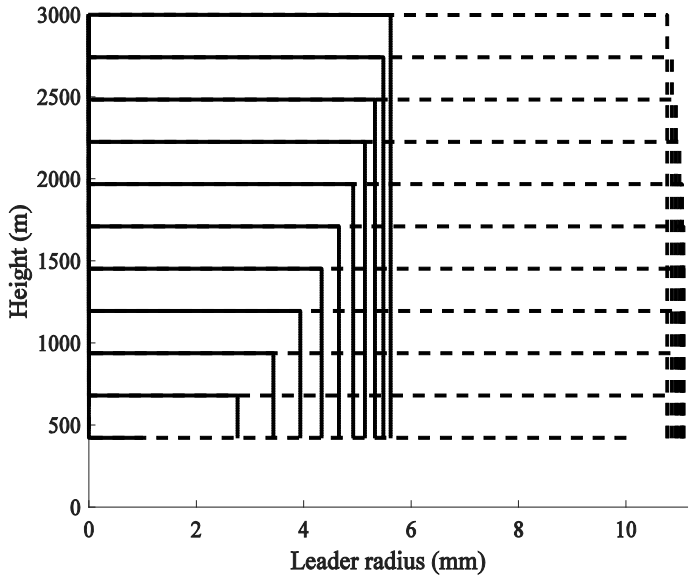

Figure 14. Leader core radius (R_L solid line) and transition layer radius (R_T dash line) versus leader tip height for Case 2 for E_{cloud} = -20 kV/m and E_{ground} = -3 kV/m.

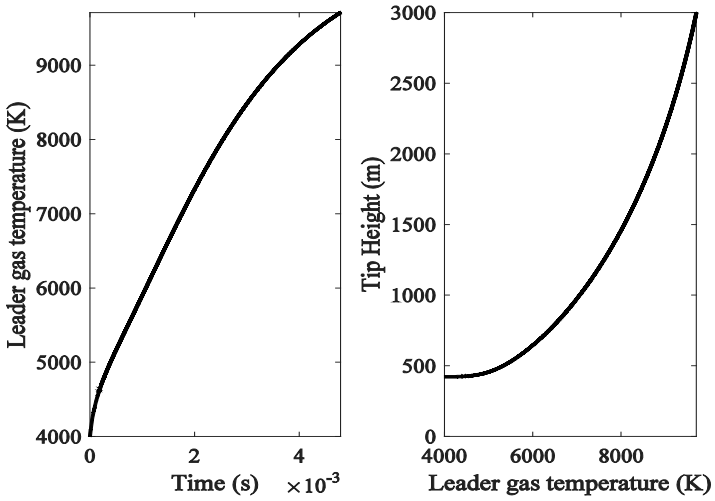

Figure 15. Leader core temperature (T_L) versus leader propagation time (left) and that versus leader tip height (right), for Case 2 for E_{cloud} = -20 kV/m and E_{ground} = -3 kV/m.

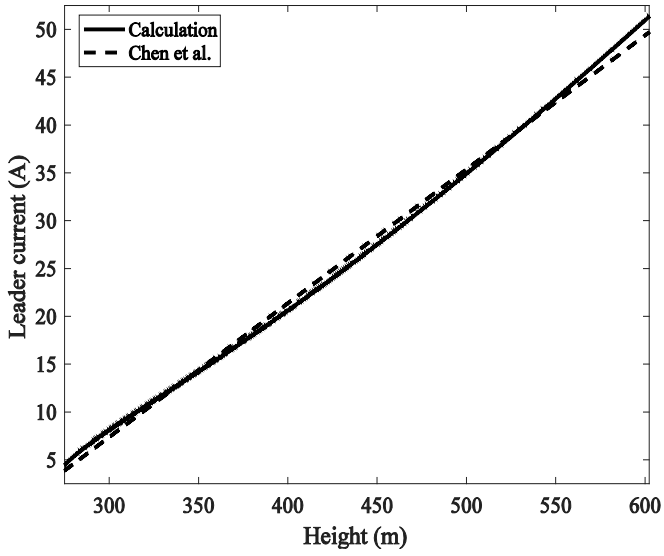

Figure 16. Comparison of the leader current evolution between modeled (solid-line) and observed (dashed-line) results for the UPL reported in *Chen et al. (2013b)*.

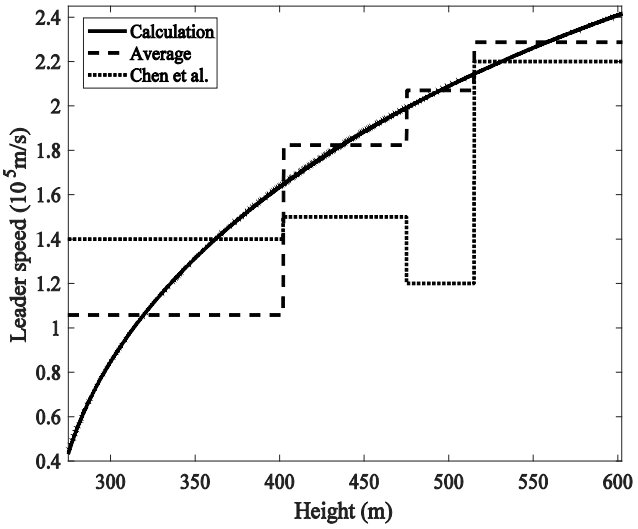

Figure 17. Comparison of the leader speed evolution between modeled (solid-line) and observed (short-dashed-line) results for the UPL reported in *Chen et al. (2013b).* Long-dashed-line is the model-based averaged speed for different channel segments in accordance with the observed result.

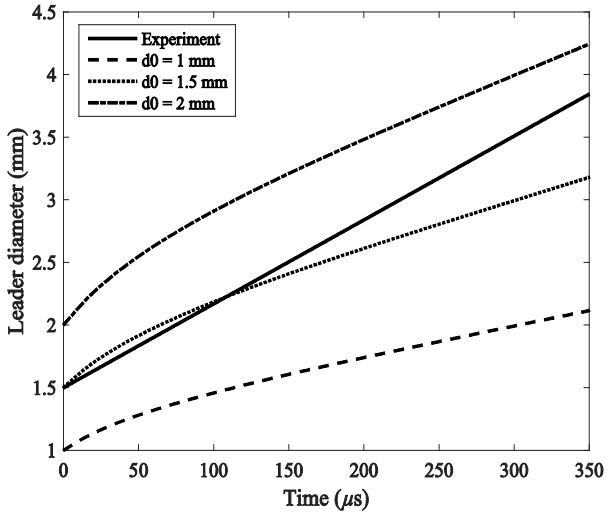

Figure 18. Evolution trends of the leader core diameter modeled with different initial values (1, 1.5 and 2 mm respectively) and that measured in lab, for the point-to-plane gap discharge reported in *Zhou et al. (2015).*

Table 1. Initial parameters for the upward positive leader simulation.

Symbol	Quantity	Value
M	Effective molar mass	73 g/mol
H	Simulation height	3000 m
E_{cloud}	Electric field due to the cloud charge	-30 to -10 kV/m
E_{C0}	Breakdown electric field at ground level	+500 kV/m
g_{L0}	Initial conductance per unit length	0.1 mS/m
R_{L0}	Initial leader core radius	1 mm (Gallimberti, 1979)
R_{T0}	Initial transition zone radius	10 mm
T_e	Electron temperature	20000 K (Gallimberti, 1979)
T_{L0}	Initial leader temperature	4000 K (Bazelyan et al., 2000)
τ_{a0}	Three-body attachment time at ground level	0.1 μs (Bazelyan et al., 2000)
τ_{d0}	Delay time at ground level	1 μs (Bazelyan et al. 2007)
η	Heat and vibrational energy lost	0.175 (Riousset et al. 2010)
$\Delta l=l_0$	Minimum leader length at ground level	0.10 m

Table 2. The minimum UPL self-triggering height versus cloud electric field (E_{cloud}) for Case 1 and Case 2 from the present model, and the triggering height versus leader stabilization field from other models.

E_{cloud} *or* $E_{stab.}$ (kV/m)	Case 1 (H_b, m)	Case 2 (H_b, m)	Rizk[1] (H_b, m)	Lalande[2] (H_b, m)	Becerra[3] (H_b, m)
-10	1191.5	1259.5	151.7	1337.5	330.6 m
-15	469.0	601.0	99.8	712.5	214.3 m
-20	252.5	410.0	73.9	290.7	157.1 m
-25	157.5	319.0	58.4	176.7	120.4 m
-30	108.0	265.0	48.0	124.0	83.7 m

[1] Rizk (1994); [2] Lalande et al. (1996); [3]Becerra and Cooray (2006b)

Table 3. Summary of simulation results for UPL traveling from its triggering height (H_b) to 3000 m high with different cloud electric field (E_{cloud}) for both Case 1 and Case 2.

Cloud Field (E_{cloud})	Leader current I_L (A) Case 1	Case 2
-10 kV/m	3.0 – 130.1	3.0 – 116.7
-15 kV/m	2.0 – 248.8	2.2 – 223.6
-20 kV/m	1.5 – 340.5	1.8 – 307.6
-25 kV/m	1.2 – 421.9	1.6 – 387.0
-30 kV/m	1.0 – 494.8	1.5 – 463.8
Cloud Field	Leader longitudinal E-field E_L (V/m) Case 1	Case 2
-10 kV/m	- 9999 – -231	-9953 – -257
-15 kV/m	-14999 – -121	-13914 – -134
-20 kV/m	-19981 – -88	-16695 – -98
-25 kV/m	-24999 – -71	-18842 – -78
-30 kV/m	-29956 – -61	-20613 – -65
Cloud Field	Leader tip line charge density λ_L (μC/m) Case 1	Case 2
-10 kV/m	147.4 – 247.9	144.1 – 236.7
-15 kV/m	80.7 – 368.1	78.6 – 345.6
-20 kV/m	59.9 – 494.9	62.4 – 459.1
-25 kV/m	48.8 – 624.9	54.5 – 574.0
-30 kV/m	41.5 – 757.3	49.6 – 690.0
Cloud Field	Leader tip corona sheath radius R_C (m) Case 1	Case 2
-10 kV/m	0.203 – 12.74	0.211 – 12.16
-15 kV/m	0.136 – 18.91	0.146 – 17.76
-20 kV/m	0.120 – 25.43	0.131 – 23.59
-25 kV/m	0.114 – 32.11	0.125 – 29.49
-30 kV/m	0.111 – 38.91	0.121 – 35.45
Cloud Field	Leader propagation speed v_L (10^4 m/s) Case 1	Case 2
-10 kV/m	1.0 – 52.5	1.0 – 49.3
-15 kV/m	1.0 – 69.5	1.0 – 66.1
-20 kV/m	1.0 – 72.9	1.0 – 69.8
-25 kV/m	1.0 – 73.3	1.0 – 71.3
-30 kV/m	1.0 – 72.7	1.0 – 71.9
Cloud Field	Leader conductance g_L (mS/m) Case 1	Case 2
-10 kV/m	10 – 564	10 – 454
-15 kV/m	10 – 2063	10 – 1667
-20 kV/m	10 – 3864	10 – 3154
-25 kV/m	10 – 5934	10 – 4992
-30 kV/m	10 – 8160	10 – 7169
Cloud Field	Leader core radius R_L (mm) Case 1	Case 2
-10 kV/m	1 – 3.5	1 – 4.1
-15 kV/m	1 – 5.0	1 – 5.1
-20 kV/m	1 – 6.1	1 – 5.6
-25 kV/m	1 – 7.1	1 – 6.1
-30 kV/m	1 – 7.9	1 – 6.5

1